IEEE Open Journal of Vehicular Technology

Received 28 August 2024; accepted 11 September 2024. Date of publication 18 September 2024;
date of current version 5 November 2024. The review of this article was coordinated by Editor Chong Han.

Digital Object Identifier 10.1109/OJVT.2024.3464349

Software-Defined Radio-Based IEEE 802.15.4 SUN FSK Evaluation Platform for Highly Mobile Environments

JAESEOK LIM, KEITO NAKURA, SHOTA MORI (Member, IEEE), AND HIROSHI HARADA (Senior Member, IEEE)

Graduate School of Informatics, Kyoto University, Kyoto 606-8501, Japan

CORRESPONDING AUTHOR: HIROSHI HARADA (e-mail: hiroshi.harada@i.kyoto-u.ac.jp).

This work was supported in part by National Institute of Information and Communications Technology (NICT) in Japan under Grant JPJ012368C05101 and in part by the Ministry of Internal Affairs and Communications (MIC) in Japan under Grant JPJ000254. An earlier version of this paper was presented in part at the 9th IEEE World Forum on Internet of Things, Aveiro, Portugal, Oct. 2023 [DOI: 10.1109/WF-IoT58464.2023.10539489].

ABSTRACT IEEE 802.15.4 smart utility network (SUN) frequency-shift keying (FSK) has attracted considerable attention as a wireless communication standard designed for use in essential applications required by Internet of Things (IoT) systems. However, longer transmission distances in highly mobile environments are required to support various applications in next-generation IoT systems, such as vehicle-to-everything, automated driving, and drone control systems. Although research on wide-area, highly mobile communications has been conducted via computer simulations, an experimental evaluation platform for further research has not been developed. In this study, we developed an experimental evaluation platform for SUN FSK in very high frequency bands. The developed platform comprises a signal generator-based transmitter and a software-defined radio-based receiver. It was proven to be capable of transmitting a power of $\geq$5 W through a power amplifier and was suitable for laboratory and field experiments. In addition, we developed received signal processing methods, including a packet detection method and a channel estimation method, which were designed to achieve wide-area, highly mobile communication. In laboratory experiments, the packet error rate characteristics required by IEEE 802.15.4 were achieved even at a transmission distance of $>$10 km at vehicular speeds of several tens of km/h.

INDEX TERMS 802.15.4, IoT, mobile, software-defined radio, Wi-SUN, FSK, VHF.

I. INTRODUCTION

In recent years, the range of wireless communication applications in various aspects of society has expanded rapidly. The necessity of gathering and transmitting data in diverse scenarios for next-generation communication systems has heightened the significance of the wireless Internet of Things (IoT), which connects all types of objects to the Internet and allows communication between them [1].

The wireless smart utility network (Wi-SUN) has attracted considerable attention as a wireless communication standard designed for use in essential applications required by the next-generation wireless IoT system, including sensor array networks and smart metering systems [2], [3]. It utilizes the physical (PHY) layer and medium access control (MAC) layer standardized by IEEE 802.15.4-2015, is called the smart utility network (SUN), and has multiple technical specifications that are suitable for various applications [4]. In Japan, a representative Wi-SUN system application is a smart metering system [2], which primarily employs the SUN frequency-shift keying (FSK) and sub-1 GHz band. SUN FSK is suitable for the transmission of numerical and image data with a bitrate range of up to several hundred kbps and a coverage radius of approximately 2 km per base station. It offers several advantages in the context of IoT systems, including simple signal processing, low power consumption, and a narrow bandwidth of several hundred kilohertz per channel. Fundamental evaluation and field experiments with integrated circuits (ICs) were conducted with a transmission power of 20 mW, and

SUN FSK achieved a transmission distance of several hundred meters in the ultrahigh-frequency (UHF) band [5].

However, longer transmission distances in highly mobile environments are required to support various applications of next-generation IoT systems, such as vehicle-to-everything (V2X), automated driving, and drone control systems. For example, the introduction of a low-power wide area (LPWA) is being considered in next-generation V2X, and a transmission distance of >10 km at a data rate of several hundred bps to several hundred kbps is expected [6]. Furthermore, the Wi-SUN system is expected to achieve a vehicular speed of 40–80 km/h as a wide-area mobile communication, with a data rate of several hundred kbps or more, to collect sensor data, transmit videos and images from vehicles, and control vehicles [1]. Consequently, a novel IoT system that can transmit videos and images at a higher data rate than the LPWA while satisfying a transmission distance of 10 km and vehicular speed of 80 km/h is required.

To achieve wide-area, highly mobile communications, a novel SUN FSK system was proposed [7] that incorporates the following modifications: utilization of the very high frequency (VHF) band, stronger forward error correction (FEC) encoding, an increased interleaving size, two-branch spatial diversity reception, and soft-decision demodulation based on cross-correlation. The utilization of the VHF band permits a longer transmission distance and a reduction in the Doppler frequency, which mitigates the impact of fading in mobile communications. The introduction of a convolutional code with a constraint length of 7, which is utilized in SUN orthogonal frequency-division multiplexing (OFDM), and the larger interleaving size provide a more robust FEC than the traditional SUN FSK system. Additionally, two-branch spatial diversity reception and soft-decision demodulation allow wireless mobile communication in multipath fading environments in urban areas, as well as in fading models in rural areas, where long-delay (>20 μs) waves are present.

A comparison between the proposed SUN FSK system and the existing SUN FSK system is also presented in [7], demonstrating the effectiveness of the proposed SUN FSK system. However, the proposed receiver signal processing has only been evaluated using computer simulations, and to the best of our knowledge, there is no experimental evaluation platform for SUN FSK in the VHF band. Thus, for further research on SUN FSK, including laboratory and field experiments, the development of an experimental evaluation platform based on software-defined radio (SDR) receivers that permit flexible modification of the functions and parameters of the transmitter and receiver is required. This is analogous to the approach adopted by IEEE 802.22 [8], a 5th generation (5G) mobile communication new radio [9], and SUN OFDM [10].

To meet the aforementioned requirements, this study extends the work reported in [7]. On the basis of the platform developed in [10], we developed a platform for experimental evaluation that allows transmission experiments of PHY-layer packets compliant with IEEE 802.15.4 SUN FSK at various power levels, which change during high-speed (e.g., 80 km/h) travel. The experimental evaluation platform consists of a signal generator (SG)-based transmitter and an SDR-based receiver. The SG-based transmitter can transmit arbitrary signals through the MATLAB-controlled SG. The power amplifier can provide a high output power that is suitable for both laboratory and field experiments. An SDR-based receiver can perform flexible software-defined signal processing of a digital baseband (BB) signal.

For signal processing, we included FEC coding, which is more powerful than the current IEEE 802.15.4 SUN-FEC, cross-correlation-based soft-decision decoding, and interleaving size expansion [7], in the experimental evaluation platform. Furthermore, to conduct asynchronous experiments at the transmitter and receiver, it is necessary to implement a synchronization method for the received signal on an SDR-based experimental platform. In contrast to IEEE 802.22 and the new 5G mobile communication radio, SUN FSK is a packet-based communication system. Thus, a packet detection method that allows synchronization—even in a highly mobile multipath fading environment with long-delay waves—should be implemented on the evaluation platform. In this study, a packet detection method for SUN FSK was proposed, evaluated via computer simulations, and implemented in an SDR-based receiver. Carrier-frequency offset (CFO) compensation is also essential for achieving high-quality reception performance. In this study, the CFO compensation method proposed in [11] was used as the basis for the experimental platform.

In the Wi-SUN system, the introduction of spatial diversity reception and maximum ratio combining (MRC) has been considered to cope with multipath fading in highly mobile environments [10], [12]. In SUN OFDM, a channel estimation method using pilot symbols was proposed to implement MRC. However, the SUN FSK does not include pilot symbols for channel estimation. Thus, a channel estimation method that does not require pilot symbols is required. In this paper, we propose a channel estimation method based on the eigenvalue decomposition (EVD) of the correlation matrix of the received FSK signals. The proposed channel estimation method is designed to be applied to a correlation matrix of arbitrary FSK signals; thus, it does not require pilot symbols.

Finally, we constructed an evaluation setup for laboratory experiments utilizing the developed platform and conducted an experimental evaluation of SUN FSK in the VHF bands as an example of the usage of the developed platform.

The communication method for mobile nodes utilizing IEEE 802.15.4 was studied in [13], [14]; however, it was designed to support low-speed mobile nodes by modifying the MAC layer protocol. Additionally, high-rate communication utilizing IEEE 802.15.4 ultra-wideband PHY-layer was studied in [15]; however, wide-area mobile communication was not covered. In vehicle-to-vehicle, mobile communication utilizing IEEE 802.15.4 was studied [16]; however, it also did not cover PHY-layer research for wide-area communication. Furthermore, SUN FSK was not utilized in all of the aforementioned studies. For SUN, the construction of a

"large-scale IoT network" with Wi-SUN field area network has been discussed [17]. It demonstrates that the proposed SUN FSK system can be extended to a large-scale IoT network or a heavy network traffic condition.

To the best of our knowledge, no previous study has developed a receiver scheme for a wide-area highly mobile communication system by modifying the PHY-layer receiver function and implementing it in an experimental evaluation platform.

The key contributions of this study are summarized as follows:

- We developed an experimental evaluation platform for SUN FSK in the VHF band based on the platform developed in [10]. The developed platform comprises an SG-based transmitter and an SDR-based receiver. It was proven to be capable of transmitting a power of ≥ 5 W through a power amplifier and was suitable for laboratory and field experiments.
- We propose a packet detection method that can detect SUN FSK packets even in a multipath fading environment with long-delay waves at a vehicular speed of 80 km/h. This method was evaluated using computer simulations and introduced into the reception processing of the developed SDR-based receiver. The proposed packet detection method enables the transmission of SUN FSK packets despite the transmitter and receiver being in a blind state.
- We propose a channel estimation method based on the EVD of the correlation matrix of the received FSK signals. This method was designed to be applied to a correlation matrix of arbitrary FSK signals and does not require pilot symbols. It was introduced into the reception processing of the developed SDR-based receiver. This study clarifies the estimation of radio propagation characteristics and the diversity reception to allow packets defined in IEEE 802.15.4 SUN to be transmitted by real radio equipment.
- We constructed an evaluation setup using the developed platform and evaluated the transmission characteristics of SUN FSK with the following modifications: utilization of VHF bands, stronger FEC encoding, increased interleaving size, two-branch spatial diversity reception, and soft-decision demodulation based on cross-correlation.

The evaluation of the transmission characteristics demonstrated that SUN FSK achieved the PER required by the standard, even in highly mobile communication in a multipath fading environment with long-delay waves. Furthermore, we evaluated the maximum transmission distance for achieving the required PER.

The remainder of this paper is organized as follows. Section II describes the PHY-layer configuration of SUN FSK. Section III describes the configuration of the SUN FSK experimental evaluation platform. In Section IV, a packet detection method for received BB signal processing is proposed and evaluated via computer simulations. Section V presents the evaluation of the PER characteristics and transmission distance using the experimental evaluation platform. Finally, Section VI concludes the paper.

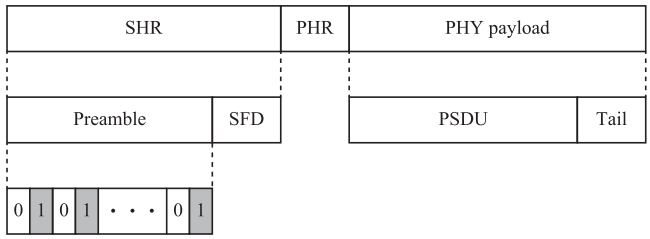

FIGURE 1. PHY-frame configuration of SUN FSK.

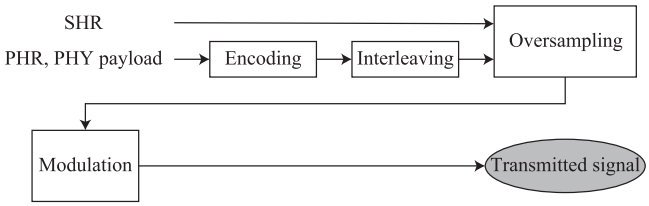

FIGURE 2. Transmitter configuration of SUN FSK.

II. IEEE 802.15.4 SUN FSK

A. OVERVIEW

This section presents the framework of the IEEE 802.15.4 SUN FSK PHY layer. The PHY-layer convergence protocol data unit (PPDU) of the IEEE 802.15.4 SUN FSK comprises a synchronization header (SHR), PHY payload, and PHY header (PHR). Fig. 1 shows the PHY-frame format of IEEE 802.15.4 SUN FSK [1].

SHR comprises a preamble and a start-frame delimiter (SFD) sequence. The preamble sequence comprises a repeating sequence of 4 to 1000 binary octets alternating between 0 and 1, such as "010101," which is used for packet detection and CFO compensation. The SFD is a two-octet sequence used for the identification of FEC information and frame synchronization. The receiver is aware of the SHR.

The PHR is a two-octet sequence that contains the control information of the frame and the PHY payload. This indicates whether the entire packet is transmitted at a single data rate using a single modulation scheme, the length of the PHY-layer convergence protocol service data unit (PSDU), the frame check sequence (FCS) field, and data whitening included in the PHY payload.

The PHY payload comprises the PSDU and tail bit for Viterbi decoding.

B. TRANSMITTER AND RECEIVER CONFIGURATIONS

The transmitter configuration of SUN FSK is shown in Fig. 2. First, convolutional coding and interleaving are applied to the PHR and PHY payloads. In this study, we utilized convolutional code with a constraint length of 7 and code rate of 1/2, which is employed in SUN OFDM [4]. An interleaving

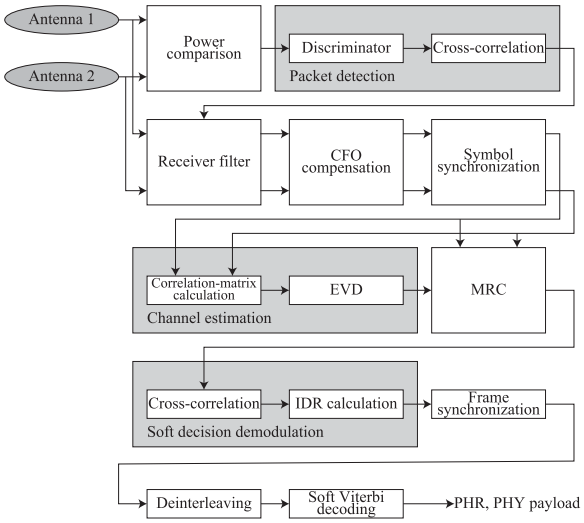

FIGURE 3. Receiver configuration of SUN FSK.

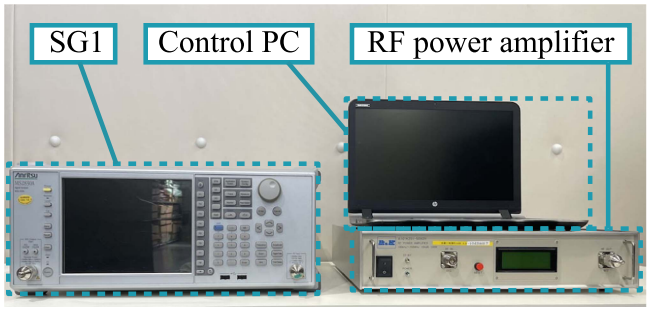

FIGURE 4. SG-based transmitter configuration of the developed platform.

TABLE 1. Equipment of SG-based Transmitter

Equipment	Product model
SG1	MS2830A, Anritsu
RF power amplifier	A101K251-5050R, R&K
Control PC	Probook 450 G3, HP (Intel Core i7-6500U CPU, 8192 MB RAM)

size equal to the lengths of the PHR and PHY payloads is employed to reduce the burst errors caused by multipath fading. The entire packet is oversampled and modulated using 2-Gaussian frequency-shift keying (GFSK).

The receiver configuration of SUN FSK is shown in Fig. 3. First, the receiver compares the powers of the two digital BB signals received from each antenna. Subsequently, the received digital BB signal from the antenna with the higher received power is subjected to packet detection to delimitate where the frame begins. In packet detection, the discriminator computes the phase shift of each symbol, whereas the correlator performs a cross-correlation between the phase shift of the received signal and that of the ideal SHR sequence. After packet detection, the received signal is filtered using a Gaussian filter. In this study, a Gaussian filter with a bandwidth–time product (BT) of 0.5 was utilized, which is equivalent to that of UHF-band Wi-SUN in Japan [4]. Following Gaussian filtering, a preamble sequence is utilized for CFO compensation and symbol synchronization [11], [18]. Subsequently, channel estimation is performed on the CFO-compensated signal [7]. The channel characteristics are estimated using the EVD of the correlation matrix of the received signal, given that the PHY-layer packet of SUN FSK does not contain a pilot symbol for channel estimation. To combine the signals from different antennas, MRC is performed using an estimated channel. Subsequently, the combined signal is subjected to soft-decision demodulation based on cross-correlation [7], [19]. After frame synchronization has been performed on the demodulated data, the PHR and PHY payloads are subjected to deinterleaving and soft Viterbi decoding.

III. SUN FSK EXPERIMENTAL EVALUATION PLATFORM

This section presents the SUN FSK experimental evaluation platform, which employs a development approach analogous to those described in [8], [9], [10]. The developed platform comprises an SG-based transmitter and an SDR-based receiver.

A. SG-BASED TRANSMITTER CONFIGURATION

The configuration of the SG-based transmitter is illustrated in Fig. 4. The equipment used for the transmitter is presented in Table 1. The transmitter comprises an SG1 (MS-2830A, Anritsu), a radiofrequency (RF) power amplifier (A101K251-5050R, R&K), and a control PC (Probook 450 G3, HP).

A digital BB signal is generated using MATLAB on a control PC, as described in Section II-B. Subsequently, the BB signal is transmitted to the SG via a LAN cable. The SG covers a frequency range of 250 kHz to 6 GHz and RF vector modulation bandwidths of up to 120 MHz. In the SG, the BB signals are converted into RF signals using a digital-to-analog converter (DAC). The SG supports IQ data waveform resolutions of 14, 15, and 16 bits [20]. The output signal of the SG is connected to a power amplifier via an RF coaxial cable.

B. SDR-BASED RECEIVER CONFIGURATION

The configuration of the SDR-based receiver is shown in Fig. 5. The equipment used in the SDR-based receiver is presented in Table 2. The SDR-based receiver comprises two RF modules (5791, National Instruments (NI)), two field-programmable gate array (FPGA) modules (PXIe-7975R, NI), a data-storage module (HDD-8261, NI), a synchronization module (PXIe-6674T, NI), and a chassis (PXIe-1082, NI). The 10-MHz oven-controlled crystal oscillator (OCXO) clock signal with an accuracy of ± 80 ppb from the synchronization module is shared with all modules over the local bus of the chassis [21].

The RF modules receive an RF signal and downconvert it into a digital BB signal using a 14-bit analog-to-digital converter (ADC) [22]. The 14-bit signal is converted into a

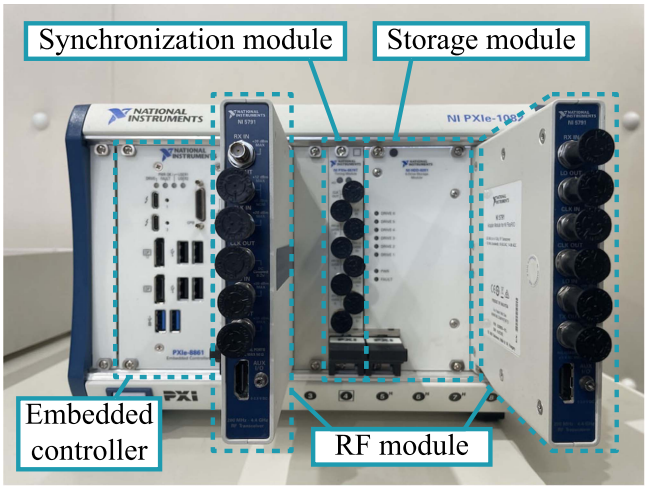

FIGURE 5. SDR-based receiver configuration of the developed platform.

TABLE 2. Equipment of SDR-Based Receiver

Equipment	Product model
Chassis	PXIe-1082, NI
Embedded controller	PXIe-8861, NI
RF module1	5791, NI
RF module2	5791, NI
Synchronization module	PXIe-6674T, NI
FPGA module1	PXIe-7975R, NI
FPGA module2	PXIe-7975R, NI
Storage module	HDD-8261, NI
BB signal processor	MATLAB 2024a, Mathworks

16-bit signal by the FPGA modules and stored as a technical data management streaming (TDMS) file [23]. Additionally, the time index and vertical range of the received signal are stored as a comma-separated value (CSV) file.

The reception processing of the received digital BB signals, which was outlined in Section II-B, is conducted using MATLAB. When a TDMS file is read in MATLAB, the vertical range of the received BB signal is compensated by referencing the corresponding CSV file. All the reception processes are software-based, allowing flexible modification of reception processing.

IV. PROPOSED RECEPTION PROCESSING METHOD

This section explains the reception processing employed in the SDR: packet detection, symbol synchronization, frame synchronization, CFO compensation, channel estimation, MRC, and soft-decision demodulation.

A. PACKET DETECTION

The SDR implements a packet detection scheme that utilizes the SHR of the received BB signal. In calculating the cross-correlation of the IQ waveform between the ideal SHR and received signal, it was observed that a constant floor error occurred in the multipath fading channel, even in the high-signal-to-noise ratio (SNR) region. This is because amplitude fluctuations resulting from fading affect the cross-correlation of the IQ waveforms. Herein, we propose a packet detection method based on the cross-correlation between the phase shift of the ideal SHR and the phase shift of the received signal. The cross-correlation between the phase shift of the ideal SHR and that of the received signal is expressed as follows:

$$R_{\mathrm{PD}}[k] = \sum_{n=1}^{N_{\mathrm{SHR}}} \Delta\theta_{\mathrm{SHR}}[n]\, \Delta\theta_{\mathrm{rx}}[n+k-1], \tag{1}$$

where k and n are the sample indices of the BB signal, $\Delta\theta_{\mathrm{SHR}}[n]$ represents the phase shift between the n-th and $(n+1)$-th digital samples of the SHR, $\Delta\theta_{\mathrm{rx}}[k]$ represents the phase shift between the k-th and $(k+1)$-th digital samples of the received signal, and N_{SHR} represents the sample length of the SHR. The packet detection point k_{PD} can be calculated as follows:

$$k_{\mathrm{PD}} = \arg\max_{k} \left(R_{\mathrm{PD}}[k]\right) - N_{\mathrm{SHR}} + 1. \tag{2}$$

B. SYMBOL AND FRAME SYNCHRONIZATION

The symbol synchronization point, which represents the boundary between the symbols of oversampled signals, can be identified by detecting the extremum phase shift of the preamble sequence [18]. Let the preamble of the received BB signal be $r^{\mathrm{pre}}[k]$, and let the oversample factor be m. Because the preamble is a periodic pattern of 0 s and 1 s, by dividing the preamble into intervals of 2 m samples and calculating the arithmetic average between each interval, it is possible to obtain a preamble in which the influence of additive white Gaussian noise (AWGN) is reduced. For the in-phase components, the following equation is derived:

$$r_{\mathrm{ich}}^{\mathrm{ave}}[k] = \frac{1}{N_1} \sum_{n=1}^{N_1} r_{\mathrm{ich}}^{\mathrm{pre}}[2m(n-1)+k]. \tag{3}$$

N_1 determines the number of intervals used to calculate the average value. The quadrature components are eligible for the same signal processing. The averaged preamble of the quadrature components is denoted as $r_{\mathrm{qch}}^{\mathrm{ave}}[k]$. The phase shift is calculated from the arithmetic average of the signals. For symbol synchronization, the sample point with the maximum phase value is used as the symbol synchronization point k_{symbol}.

$$k_{\mathrm{symbol}} = \arg\max_{k} \tan^{-1}\left(\frac{r_{\mathrm{qch}}^{\mathrm{ave}}[k]}{r_{\mathrm{ich}}^{\mathrm{ave}}[k]}\right). \tag{4}$$

The preamble sequence utilized for actual symbol synchronization is 1 or 2 bytes in length.

Subsequently, frame synchronization was conducted to ascertain the indices of the PHR and PSDU. In this study, a frame synchronization method was employed by utilizing the cross-correlation between the demodulated signal and the ideal SFD [3]. The frame synchronization point k_{frame} can be

calculated as follows:

$$R_{\text{frame}}[k] = \sum_{n=1}^{N_2} r_{\text{d}}[n+k-1]\,\text{SFD}[n], \tag{5}$$

$$k_{\text{frame}} = \{k | R_{\text{frame}}[k] \geq \alpha\}, \tag{6}$$

where r_{d} represents the demodulated signal; SFD represents the ideal SFD sequence; N_2 represents the bit length of the SFD, which corresponds to 16 bits in the case of 2-FSK; and α represents the threshold value.

C. CFO COMPENSATION

In actual Wi-SUN modules, low-cost and low-precision local oscillators are integrated to achieve the objectives of miniaturization, high power efficiency, and cost reduction. Consequently, a CFO of approximately 20 ppm is produced relative to the carrier frequency in the UHF band [24].

To estimate and compensate for the CFO, a CFO compensation method utilizing a moving-average low-pass filter (LPF) was developed [11]. As outlined in Section II-A, the preamble sequence of SUN FSK comprises an alternating pattern of 0s and 1s; thus, it is possible to approximate the in-phase component $r_{\text{ich}}^{\text{pre}}$ and quadrature component $r_{\text{qch}}^{\text{pre}}$ with sinusoidal waves as follows:

$$r_{\text{ich}}^{\text{pre}}(t) \cong A_{\text{ich}}^{\text{pre}} \cos \pi R t, \tag{7}$$

$$r_{\text{qch}}^{\text{pre}}(t) \cong A_{\text{qch}}^{\text{pre}} \cos 2\pi R t - B_{\text{qch}}, \tag{8}$$

where $A_{\text{ich}}^{\text{pre}}$ and $A_{\text{qch}}^{\text{pre}}$ represent the amplitudes of the components, B_{qch} is a positive constant, R represents the symbol rate, and f_{CFO} represents the CFO. Given that the occurrence of CFO is equal to the product of the rotation matrix of f_{CFO}, the in-phase component with CFO $\tilde{r}_{\text{ich}}^{\text{pre}}(t)$ can be expressed as

$$\tilde{r}_{\text{ich}}^{\text{pre}}(t) = r_{\text{ich}}^{\text{pre}}(t) \cos 2\pi f_{\text{CFO}} t - r_{\text{qch}}^{\text{pre}}(t) \sin 2\pi f_{\text{CFO}} t. \tag{9}$$

If the approximations of $r_{\text{ich}}^{\text{pre}}$ and $r_{\text{qch}}^{\text{pre}}$ are substituted, following equation is obtained:

$$\begin{aligned}\tilde{r}_{\text{ich}}^{\text{pre}}(t) = {} & \frac{A_{\text{ich}}^{\text{pre}}}{2}\left\{\cos 2\pi\left(\frac{R}{2}+f_{\text{CFO}}\right)t \right. \\ & \left. + \cos 2\pi\left(\frac{R}{2}-f_{\text{CFO}}\right)t\right\} \\ & - \frac{A_{\text{qch}}^{\text{pre}}}{2}\{\sin 2\pi(R+f_{\text{CFO}})t \\ & + \sin 2\pi(R-f_{\text{CFO}})t\} + B\sin 2\pi f_{\text{CFO}} t. \end{aligned} \tag{10}$$

Thus, when the sampling rate is sufficiently large relative to the CFO, the CFO can be estimated using the LPF.

The CFO detection method employed in this study utilizes a moving-average filter as an LPF. The frequency response of the moving-average filter is determined as follows:

$$H\left(e^{\text{j}\omega T_{\text{sp}}}\right) = e^{-\text{j}\frac{S_{\text{ave}}-1}{2}\omega T_{\text{sp}}} \frac{1}{S_{\text{ave}}} \frac{\sin\left(\frac{S_{\text{ave}}}{2}\omega T_{\text{sp}}\right)}{\sin\left(\frac{1}{2}\omega T_{\text{sp}}\right)}, \tag{11}$$

$$\left|H\left(e^{\text{j}\omega T_{\text{sp}}}\right)\right| = \frac{1}{S_{\text{ave}}} \left|\frac{\sin\left(\frac{S_{\text{ave}}}{2}\omega T_{\text{sp}}\right)}{\sin\left(\frac{1}{2}\omega T_{\text{sp}}\right)}\right|, \tag{12}$$

where S_{ave} represents the number of sample points used to calculate the moving average, T_{sp} represents the sample time, and ω represents the angular frequency of an input signal. Increasing S_{ave} results in a narrower dynamic range of the moving-average filter, while increasing the frequency resolution. Furthermore, using a longer time range for the moving-average operation enhances the cancellation of AWGN components. With the appropriate setting of S_{ave}, it is possible to cope with a wide range of CFO values.

D. CHANNEL ESTIMATION

In general, channel estimation is needed to manage multipath fading. However, the SUN FSK system does not include pilot symbols for channel estimation. Channel estimation without pilot symbols is necessary to ensure compatibility with conventional SUN FSK transceivers.

We propose a channel estimation method based on the EVD of the correlation matrix of the received FSK signals that does not require pilot symbols. The fundamental principle of the method is that the eigenvectors corresponding to the largest eigenvalues of the correlation matrix of the channel characteristics are identical to the channel characteristics themselves [25]. In the case of SUN FSK, because the amplitude of the symbol is constant, the transmitted signal can be separated into constant terms when the correlation matrix of the received signal is calculated. Consequently, the channel characteristics can be calculated using the correlation matrix of the received signal.

The diversity reception specified in the SUN FSK standard is a two-branch single-input multiple-output (SIMO) system. The transmission signal, the received signal from each antenna, and the received signal from discrete time index 1 to K are denoted as $s[k]$, $\boldsymbol{x}[k] = [x_1[k],\ x_2[k]]^{\text{T}}$, and $\boldsymbol{X} = [\boldsymbol{x}[1],\ \boldsymbol{x}[2], \cdots,\ \boldsymbol{x}[K]]$, respectively, where K represents the estimated frame length, and $(\cdot)^{\text{T}}$ denotes the transpose. The correlation matrix of the received signal is expressed as follows:

$$\boldsymbol{X}\boldsymbol{X}^{\text{H}} = \begin{bmatrix} \sum_{i=1}^{K} x_1[i] x_1^*[i] & \sum_{i=1}^{K} x_1[i] x_2^*[i] \\ \sum_{i=1}^{K} x_2[i] x_1^*[i] & \sum_{i=1}^{K} x_2[i] x_2^*[i] \end{bmatrix}, \tag{13}$$

where $(\cdot)^*$ denotes the complex conjugate, and $(\cdot)^{\text{H}}$ denotes the Hermitian transpose. Assuming that the channel characteristics remain consistent throughout the estimated frame duration and that the propagation channel characteristics of both antennas are represented by $\boldsymbol{h} = [h_1,\ h_2]^{\text{T}}$, the received signal is expressed as $\boldsymbol{x}[k] = [h_1 s[k],\ h_2 s[k]]^{\text{T}}$. Because $s[k]s^*[k] = 1$ in the case of FSK, the correlation matrix of the received signal can be obtained as

$$\boldsymbol{X}\boldsymbol{X}^{\text{H}} \cong K\boldsymbol{h}\boldsymbol{h}^{\text{H}}. \tag{14}$$

From (10), it is feasible to derive the radio propagation channel characteristics by assessing the largest eigenvalue

and the corresponding eigenvectors of the correlation matrix generated from the received signal.

Therefore, let the maximum eigenvalue of the correlation matrix of the received signal be λ, and let the corresponding eigen vector be $\boldsymbol{v}$. Then, the estimated channel characteristics $\hat{\boldsymbol{h}} = [\hat{h}_1,\ \hat{h}_2]^{\mathrm{T}}$ are estimated as follows:

$$\hat{\boldsymbol{h}} = \sqrt{\lambda}\boldsymbol{v}. \tag{15}$$

E. MRC

In this study, two RF modules were utilized as separate antennas to implement two-branch spatial diversity reception. MRC involves combining the received signals from multiple independent antennas after multiplying them by appropriate weight vectors. The SNR of the combined signal is equal to the sum of the SNRs of the antennas, and the weight vector is the complex conjugate of the channel characteristics [26].

Using the estimated channel, the combined signal y is obtained as follows:

$$y = \frac{x_1\hat{h}_1^* + x_2\hat{h}_2^*}{\left|\hat{h}_1\right|^2 + \left|\hat{h}_2\right|^2}. \tag{16}$$

F. SOFT-DECISION DEMODULATION

In this study, we utilized the soft-decision demodulation method for FSK signals, employing cross-correlation with quantized sinusoidal waves, as proposed in [7].

The frequency spectrum of each FSK symbol exhibits a frequency deviation of $m_{\mathrm{m}}R$, where m_{m} represents the modulation index. Once the received signal has been separated into individual symbols using the symbol synchronization point, a soft decision can be made by calculating the internal division ratio (IDR) or log-power ratio (LPR) of the power at each frequency deviation via a fast Fourier transform (FFT) [19].

Nevertheless, with regard to circuit size and power consumption, it is not optimal to utilize the FFT for soft decisions in the case of SUN FSK, compared with hard decisions. Moreover, increasing the FFT size to enhance the frequency resolution increases the computational and circuit complexity.

Because only the power of each frequency deviation is used for the calculation of the IDR, only a few rows of FFT (e.g., in the case of MFSK, M rows) are utilized. Consequently, it is unnecessary to calculate the entire FFT matrix; only the row corresponding to each frequency deviation must be calculated, which implies that a cross-correlation calculation with a sinusoidal wave is required. The proposed soft-decision demodulation method entails identifying a row in the FFT matrix that corresponds to the frequency deviation of each symbol and then performing only the requisite calculations for these rows. Below, we present an example of a soft demodulation method design in the case of 2-GFSK modulation, which is the most prevalent form of SUN FSK.

1) Given that the frequency deviation is $m_{\mathrm{m}}R$, the center frequency of the frequency spectrum of each symbol becomes $\pm m_{\mathrm{m}}R/2$. Substitution of the sample time T_{sp} and the oversample factor m yields $\pm m_{\mathrm{m}}R/2 = \pm m_{\mathrm{m}}/2mT_{\mathrm{sp}}$.
2) The power at the frequency deviation of each symbol can be determined by calculating discrete cross-correlation between the received signal and a discrete sinusoidal matrix with a sampling rate of $1/T_{\mathrm{sp}}$ and frequency of $\pm m_{\mathrm{m}}/2mT_{\mathrm{sp}}$.
3) In the proposed method, the soft-decision value of the 2-GFSK signal obtained using cross-correlation can be derived as follows:

$$P(k,\ f) = \left|\frac{\sum_{i=1}^{N_3} e^{-\mathrm{j}2\pi f T_{\mathrm{sp}}(i-1)/N_3} r[k]}{N_3}\right|^2, \tag{17}$$

$$r_{\mathrm{IDR}}[k] = \frac{P\left(k, \frac{m_{\mathrm{m}}}{2mT_{\mathrm{sp}}}\right) - P\left(k, -\frac{m_{\mathrm{m}}}{2mT_{\mathrm{sp}}}\right)}{P\left(k, \frac{m_{\mathrm{m}}}{2mT_{\mathrm{sp}}}\right) + P\left(k, -\frac{m_{\mathrm{m}}}{2mT_{\mathrm{sp}}}\right)}, \tag{18}$$

where $r[k]$ represents the k-th sample of the zero-padded received symbol, and N_3 represents the window size of cross-correlation.

In contrast to the general 2-bit quantization approach, the partitions $\{-0.5,\ 0.5\}$ are utilized in this method, with the codebook set to $\{-1,\ 0,\ 1\}$. The correlation calculation with the array quantized as $\{-1,\ 0,\ 1\}$ is equivalent to the addition and subtraction between each element. This methodology allows the calculation of cross-correlations without a multiplication. The quantized sinusoidal waves are calculated as follows:

$$S_f[i] = \left\lfloor \cos\frac{2\pi f T_{\mathrm{sp}}(i-1)}{N_3} + \frac{1}{2} \right\rfloor + \mathrm{j}\left\lfloor -\sin\frac{2\pi f T_{\mathrm{sp}}(i-1)}{N_3} + \frac{1}{2} \right\rfloor. \tag{19}$$

Accordingly, the soft-decision value is calculated using quantized sinusoidal waves, as follows:

$$\hat{P}(k,\ f) = \left|\frac{\sum_{i=1}^{N_3} S_f[i]\, r[k]}{N_3}\right|^2, \tag{20}$$

$$\hat{r}_{\mathrm{IDR}}[k] = \frac{\hat{P}\left(k, \frac{m_{\mathrm{m}}}{2mT_{\mathrm{sp}}}\right) - \hat{P}\left(k, -\frac{m_{\mathrm{m}}}{2mT_{\mathrm{sp}}}\right)}{\hat{P}\left(k, \frac{m_{\mathrm{m}}}{2mT_{\mathrm{sp}}}\right) + \hat{P}\left(k, -\frac{m_{\mathrm{m}}}{2mT_{\mathrm{sp}}}\right)}. \tag{21}$$

The calculated IDR value is employed in the soft Viterbi decoding process.

V. EVALUATION OF TRANSMISSION CHARACTERISTICS

Laboratory experiments and computer simulations were conducted to evaluate the proposed packet detection method, receiver sensitivity of the SDR-based receiver, SNR–PER characteristics, and transmission distance.

A. OVERVIEW

An evaluation setup utilizing the developed platform was constructed for the laboratory experiments, as illustrated in

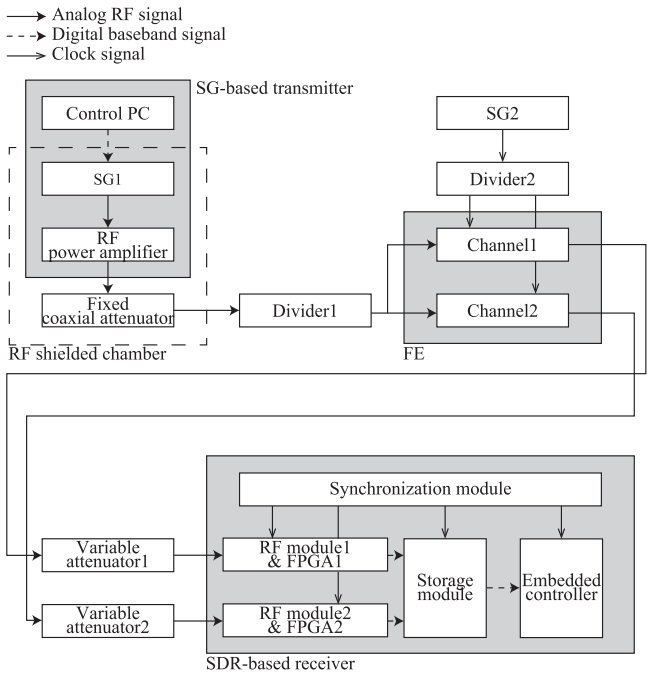

FIGURE 6. Evaluation setup for the laboratory experiments.

TABLE 3. Equipment of Evaluation Setup

Equipment	Product model
SG1	MS2830A, Anritsu
SG2	MS2830A, Anritsu
Fixed coaxial attenuator	50FHGR-150N, JFW
	BW-N30W20+, Mini Circuits
Variable attenuator	8494B, Keysight
	8496B, Keysight
RF power amplifier	A101K251-5050R, R&K
RF shielded chamber	MD-203190, MICRONIX
FE	NJZ-1600D, JRC
Divider1	PD030-0S, R&K
Divider2	PD030-0S, R&K
SDR	Chassis: PXIe-1082, NI
	Embedded controller: PXIe-8861, NI
	RF module1: 5791, NI
	RF module2: 5791, NI
	Synchronization module: PXIe-6674T, NI
	FPGA module1: PXIe-7975R, NI
	FPGA module2: PXIe-7975R, NI
	Storage module: HDD-8261, NI
BB signal processor	MATLAB 2024a, Mathworks
Control PC	Probook 450 G3, HP
	(Intel core i7-6500U CPU, 8192 MB RAM)

Fig. 6. The setup comprised an SG-based transmitter, an SDR-based receiver, an RF-shielded chamber (MD-203190, MICRONIX), a fading emulator (FE) (NJZ-1600D, JRC), SG2 (MS-2830A, Anritsu), fixed coaxial attenuators (50FHGR-150N, JFW and BW-N30W20+, Mini Circuits), variable attenuators (8494B and 8496B, Keysight), and two dividers (PD030-0S, R&K). The equipment used in the evaluation setup is presented in Table 3.

TABLE 4. Parameters Used for Simulations and Experiments

Parameters	Values
Modulation	2-GFSK
Carrier frequency	173 MHz
Bandwidth	400 kHz/channel
Bitrate	100 kbps
Sampling rate	800 ksamples/s
Modulation index	1
Gaussian filter, BT	Tx: 0.5, Rx: 0.5
Encoding	RSC FEC
	Coding rate: 1/2
Convolution code	Constraint length: 7
	Generator polynomial: 133, 171
Decoding	Soft-decision Viterbi algorithm
Packet size	Preamble: 15 octets
	SFD: 2 octets
	PHR: 2 octets
	PSDU: 250 octets
Diversity reception	AWGN channel: None
	Multipath fading channel: 2-branch MRC
S_{ave}	16
N_1	1
α	14
Estimated frame length	200
Interleaving size	4064
Number of packets	10000

The SG1 and RF power amplifiers were configured within the RF-shielded chamber to prevent the direct propagation of electromagnetic waves from the transmitter to the RF module. Fixed coaxial and variable attenuators were used for flexible power adjustment. To implement the two-branch diversity reception, the RF signal was split into two channels using a divider. Each RF signal was input into two independent channels of the FE via an RF coaxial cable. The FE model can emulate up to 12 paths by simulating two independent six-path channels. It supports frequency ranges of 70 to 340 MHz and 460 MHz to 3 GHz, a bandwidth of up to 20 MHz, and a maximum Doppler frequency of 2 kHz. The output of SG2 was divided into two channels using a divider and supplied as a clock signal for each channel of the FE. The FE output was input to each RF module of the SDR-based receiver. As described in Section III-B, the SDR-based receiver receives and downconverts the RF signal into a digital BB signal, which is then stored as TDMS and CSV files in the storage module. The digital BB signal stored in the storage module is demodulated through signal processing, as described in Section IV. A digital BB signal processor was developed using MATLAB [27]. To evaluate the SNR–PER characteristics, AWGN was added to the recorded received signals using MATLAB.

The software utilized for the computer simulations was developed in MATLAB [26]. It was based on that utilized in [7] and has been validated. As in the laboratory experiments, each packet was demodulated using the signal processing method described in Section IV.

Table 4 presents the parameters used in the computer simulations and laboratory experiments. In this study, the COST207 GSM typical urban (TU) model was utilized for TU

TABLE 5. COST207 GSM Typical Urban Model

Parameter	Path 1	Path 2	Path 3	Path 4	Path 5	Path 6
Delay (μs)	–0.2	0	0.3	1.4	2.1	4.8
Relative power (dB)	–3	0	–2	–6	–8	–10

TABLE 6. IEEE 802.22 Profile A Model

Parameter	Path 1	Path 2	Path 3	Path 4	Path 5	Path 6
Delay (μs)	0	3.0	8.0	11	13	21
Relative power (dB)	0	–7	–15	–22	–24	–19

multipath fading, and the IEEE 802.22 profile A model was utilized as a multipath fading model with long-delay (>20 μs) waves [28], [29]. The evaluation method through COST207 GSM TU and IEEE 802.22 profile A model in the VHF band has been validated through a study on V2X [6] and field experiments [30]. In [6], the transmission characteristics of a wireless communication system for V2X in the VHF band have been evaluated by computer simulation using the GSM TU and IEEE 802.22 Profile A model, as in this study. Its field experiments [30] also show that its system can achieve a transmission distance of more than 10 km in a real outdoor environment. The delay times and relative powers for the different fading models are presented in Tables 5 and 6. As for the maximum Doppler frequency, simulations and experiments were conducted at the following three vehicular speeds: 4 km/h as a walking speed and 40 and 80 km/h as vehicular speeds [3]. The PER was evaluated for the PHR and PSDU. As the required PER of SUN FSK defined by IEEE 802.15.4 SUN, PER $= 10^{-1}$ was utilized when the PSDU length was 250 octets [4].

B. EVALUATION OF PROPOSED PACKET DETECTION METHOD THROUGH COMPUTER SIMULATIONS

The packet detection method proposed in Section IV-A was evaluated using computer simulations. First, we evaluated the PER characteristics due to synchronization errors in packet detection in an AWGN channel. For the assessment of the AWGN environment, only one receiver branch was used. Thus, a reception process that excluded channel estimation and MRC was applied.

The SNR–PER characteristics in the AWGN environment when a synchronization error occurs in the packet detection step are presented in Fig. 7. The SNR–PER characteristics did not deteriorate in synchronization errors below 896 samples. This is because the receiver of SUN FSK performed frame synchronization on the demodulated signal; thus, the synchronization error occurring in the packet detection step does not affect the PER characteristics, even if a few samples of synchronization errors occur, as long as the preamble required for symbol synchronization is fully secured. In other words, the PER characteristics are affected by the total length of the preamble and the length of the preamble employed for symbol

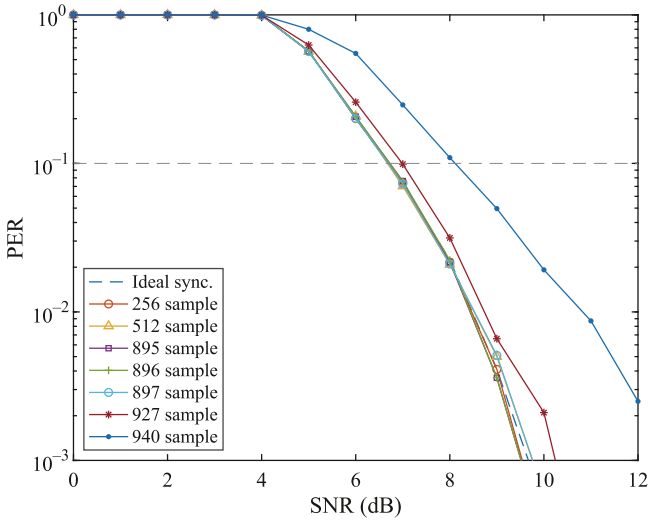

FIGURE 7. SNR–PER characteristics with synchronization errors.

synchronization rather than by the number of samples of the synchronization error.

To implement symbol synchronization, the SUN FSK receiver employs the k_{PD}-th to $(k_{\mathrm{PD}} + N_1 - 1)$-th samples of the received BB signal as a preamble sequence. Given that the length of the entire preamble is 960 samples and that the length of the preamble required for symbol synchronization is 64 samples, it is impossible to obtain the complete preamble required for symbol synchronization from the synchronization errors of the 897 samples. For synchronization errors of up to 896 samples, the 64 preamble samples required to implement symbol synchronization were fully secured, indicating PER characteristics equivalent to those for ideal synchronization. As in the cases of 927 and 940 samples, the PER characteristics gradually deteriorated after the synchronization error of sample 897. In this study, a synchronization error of <897 samples was allowed for packet detection, whereby the preamble required for symbol synchronization was fully secured.

Subsequently, the SNR–synchronization error rate (SER) characteristics of multipath fading channels were evaluated. The SNR–SER characteristics of the COST207 GSM TU model and IEEE 802.22 profile A model for vehicular speeds of 4, 40, and 80 km/h are shown in Fig. 8. The required SNR to achieve SER $= 10^{-1}$ was approximately 7.3 and 8.7 dB at a vehicular speed of 4 km/h in the COST207 GSM TU model and the IEEE 802.22 profile A model, respectively. At 40 and 80 km/h, a PER deterioration of approximately 5 dB was observed. These results indicate that the proposed packet detection method is effective, even in highly mobile communication environments.

C. RECEIVER SENSITIVITY OF SDR-BASED RECEIVER

To evaluate the receiver sensitivity of the SDR-based receiver, the received (Rx) power–PER characteristics were evaluated

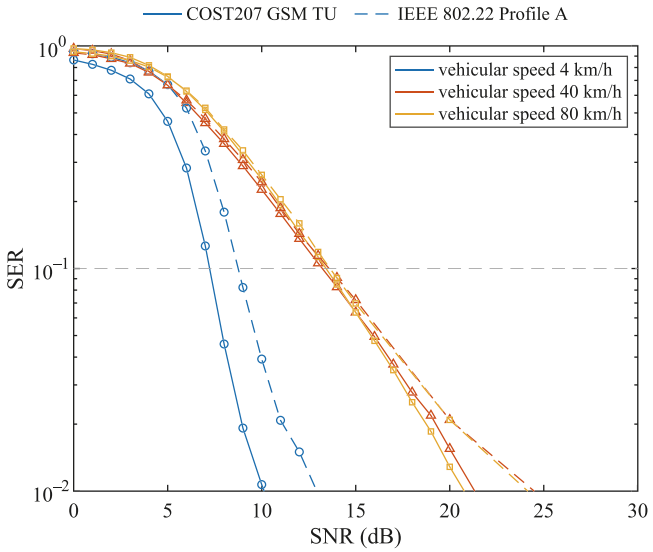

FIGURE 8. SNR–SER characteristics with synchronization errors.

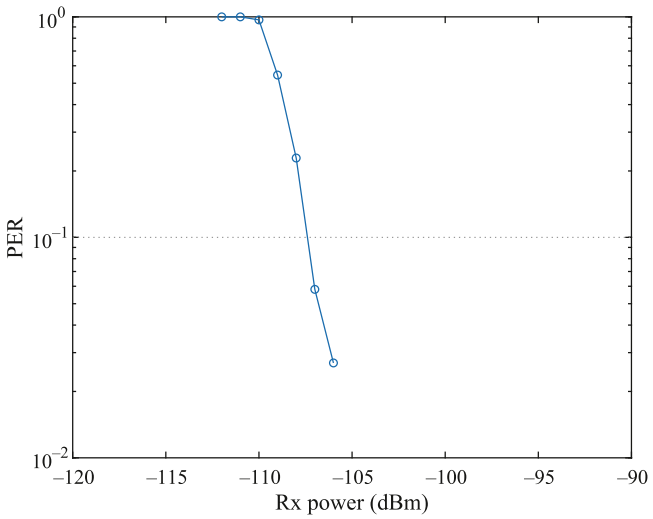

FIGURE 9. Sensitivity of the SDR-based receiver.

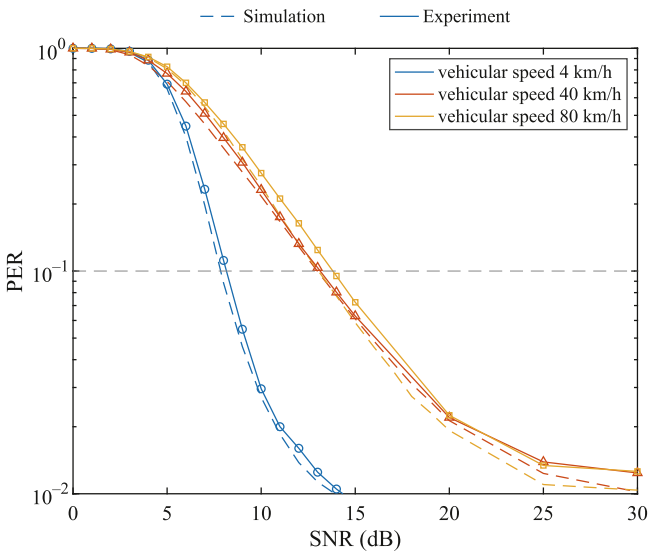

FIGURE 10. SNR–PER characteristics of the experimental evaluation platform (COST207 GSM TU model).

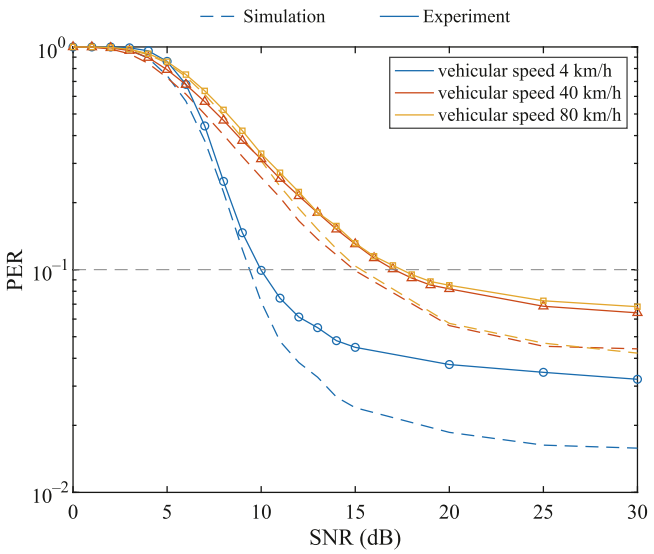

FIGURE 11. SNR–PER characteristics of the experimental evaluation platform (IEEE 802.22 profile A model).

using an experimental evaluation platform without FE, as shown in Fig. 6. The fixed coaxial attenuator was set to 60 dB, and the variable attenuator was set in the range of 0–100 dB. The input power was measured using an external spectrum analyzer (N9938B, Keysight).

Fig. 9 shows the Rx power–PER characteristics of SUN FSK. The Rx power required to achieve a PER of $<10^{-1}$ was –107 dBm. Thus, the receiver sensitivity of the SDR-based receiver was –107 dBm. The SUN FSK receiver sensitivity shall be better than S, where S, for binary modulation, is defined as follows:

$$S = \left\{ S_0 + 10\log\left(\frac{R_\mathrm{b}}{R_\mathrm{b0}}\right) \right\}, \tag{22}$$

where S_0 is –97 dBm with FEC, R_b0 is 50 kbps, and R_b is the bit rate of the SUN FSK receiver [4]. From (22), required receiver sensitivity is –90 dBm, thus the proposed SDR-based receiver meets the required receiver sensitivity. In comparison to the evaluation with ICs [5], the receiver sensitivity of the proposed SDR is improved by approximately 2 dB. This demonstrates that the proposed SDR achieves sufficient receiver sensitivity when the versatility of proposed SDR is taken into account.

D. EVALUATION IN MULTIPATH FADING ENVIRONMENT THROUGH EXPERIMENTAL EVALUATION PLATFORM

The SNR–PER characteristics of the COST207 GSM TU and IEEE 802.22 profile A models are shown in Figs. 10 and 11, respectively. For comparison, the SNR–PER characteristics

TABLE 7. Required SNR to Achieve PER = 10^{-1}

Vehicular speed [km/h]	Required SNR to achieve PER = 10^{-1} [dB]	
	COST207 GSM TU	*IEEE 802.22 profile A*
4	9	10
40	14	17
80	15	18

obtained via computer simulations are also shown. The Tx power of the SG-based transmitter was set to 37 dBm, which was the Tx power assumed in the SUN FSK field experiment in the VHF band. To minimize the quantization error, the Rx power of the FE set to –50 dBm and the reference level of the RF module was set to –30 dBm.

For the COST207 GSM TU model, the SNR–PER characteristics exhibited performance equivalent to that of the computer simulation at all vehicular speeds, satisfying the required PER of 10^{-1}. A deterioration of $\leq$0.5 dB was observed when the SNR met the required PER $= 10^{-1}$ at vehicular speeds of 4 and 40 km/h. At a vehicular speed of 80 km/h, a PER deterioration of $\leq$1.0 dB was observed.

For the IEEE 802.22 profile A model, the required PER was achieved at all vehicular speeds, and the error floor (approximately 2×10^{-2}) was increased compared with the computer simulation. A PER deterioration of $\leq$1.0 dB was observed when the SNR satisfied the required PER at a vehicular speed of 4 km/h. At vehicular speeds of 40 and 80 km/h, a PER deterioration of $\leq$2.0 dB was observed.

The SNR values required to achieve the PER are presented in Table 7. The results indicated deteriorations of $<$1 dB in the COST207 GSMTU environment and $<$2 dB in the IEEE 802.22 profile A environment relative to the computer simulations. Even in laboratory experiments, the required PER of 10^{-1} was achieved in a wide-area highly mobile environment at the data rate of 100 kbps demanded by the next-generation IoT system.

Notably, the PER deterioration between vehicular speeds of 40 and 80 km/h was significantly smaller than that between speeds of 4 and 40 km/h. At a speed of 40 km/h, the floor error reached a saturation point owing to the time-variant delay wave. Even at 80 km/h, the PER was relatively stable.

E. TRANSMISSION DISTANCE EVALUATION

To assess the transmission distance with consideration of the carrier frequency, the Okumura-Hata model was employed [3], [31]. Table 8 presents the parameters used to compute the transmission distance, which are based on those used in an evaluation of 5G in the VHF band [31]. The transmit power, transmitter antenna gain, receiver antenna gain, Boltzmann factor, temperature, bandwidth, and noise index are denoted as P_{T}, G_{T}, G_{R}, k_{B}, T, B, and F, respectively. The SNR at the receiver (dB) is expressed as follows:

$$\mathrm{SNR} = P_{\mathrm{T}} + G_{\mathrm{T}} + G_{\mathrm{R}} - L(d) - k_{\mathrm{B}}TBF, \qquad (23)$$

where $L(d)$ denotes the path loss defined in [32], which is a function of the transmission distance d. For the COST207 GSM TU model, the environments defined in [31] as metropolitan and small cities were employed. In contrast, for the IEEE 802.22 profile A model, suburban and rural areas were utilized. The Okumura-Hata model was used as a path-loss model, and the transmission distances in relation to the SNR for each fading channel were determined, as shown in Tables 9 and 10.

TABLE 8. Parameters Used for Computation of Transmission Distance

Parameter		Value
Carrier frequency		173 MHz
Bandwidth		400 kHz/channel
Transmitter	Height	60 m
	Tx power	37 dBm
	Tx antenna gain	3 dB
Receiver	Height	4 m
	Noise figure	4 dB
	Rx antenna gain	0 dB
	Temperature	300 K
Propagation model		Okumura-Hata model
Fading margin		5 dB

TABLE 9. Transmission Distance to Achieve PER = 10^{-1} (COST207 GSM TU)

Vehicular speed [km/h]	Environment	Transmission distance [km]
4	Metropolitan	16.06
	Small city	16.02
40	Metropolitan	11.36
	Small city	11.33
80	Metropolitan	10.60
	Small city	10.58

TABLE 10. Transmission Distance to Achieve PER = 10^{-1} (IEEE 802.22 Profile A)

Vehicular speed [km/h]	Environment	Transmission distance [km]
4	Suburban	23.70
	Rural	78.01
40	Suburban	14.59
	Rural	48.05
80	Suburban	13.62
	Rural	44.83

For the COST207 GSM TU model, transmission distances of 10.60 km in a metropolitan environment and 10.58 km in a small-city environment were achieved even when the vehicular speed was 80 km/h. In contrast, for the IEEE 802.22 profile A model, transmission distances of 13.62 km in a suburban environment and 44.83 km in a rural environment were achieved when the vehicular speed was 80 km/h.

The results suggest that wide-area highly mobile communication satisfying a transmission distance of $\geq$10 km at a movement speed of 80 km/h, which is required for next-generation IoT systems, is feasible in both urban and rural areas.

VI. CONCLUSION

We developed an experimental evaluation platform for SUN FSK that allows high-speed mobile communication in the VHF band. Furthermore, the platform was employed to assess the SNR–PER characteristics in a multipath fading environment. It comprises an SG-based transmitter and an SDR-based receiver. The developed platform was suitable for both field and laboratory experiments. The SG-based transmitter allows the transmission of SUN FSK signals with varying parameters, and the SDR-based receiver facilitates flexible modification of received signal processing.

Furthermore, we developed a packet detection method for asynchronous experiments between the transmitters and receivers. The SER of the proposed packet detection method was evaluated through computer simulations.

The transmission characteristics of SUN FSK in the VHF band under multipath fading channels were evaluated via computer simulations and laboratory experiments. It was found that even in a multipath fading environment with long-delay ($>$20 μs) waves in the VHF band, a transmission distance of $\geq$10 km can be achieved when the terminal is moving at a speed of 80 km/h.

In the future, we plan to conduct field experiments in diverse scenarios for next-generation IoT communication systems using the developed platform.

ACKNOWLEDGMENT

The authors would like to thank Prof. Keiichi Mizutani, Hiroko Masaki, Norichika Ohmi and Shinichi Ishiko, Kyoto University, for their valuable advice on the evaluation setup.

REFERENCES

[1] S. Popli, R. K. Jha, and S. Jain, "A survey on energy efficient narrowband Internet of Things (NBIoT): Architecture, application and challenges," *IEEE Access*, vol. 7, pp. 16739–16776, 2019.

[2] T. Kiuchi and T. Okabe, "Sensor information transmission using a smart meter communication network to monitor electric power facilities," *CIGRE Colloq. Study Committee D2*, Helsinki, Finland, Jun. 2019.

[3] H. Harada, K. Mizutani, J. Fujiwara, K. Mochizuki, K. Obata, and R. Okumura, "IEEE 802.15.4g based WI-SUN communication systems," *IEICE Trans. Commun.*, vol. E100-B, no. 7, pp. 1032–1043, Jul. 2017.

[4] *IEEE Standard for Low-Rate Wireless Networks*, IEEE Standard 802.15.4-2015, Apr. 2016.

[5] Y. Xiang, R. Okumura, K. Mizutani, and H. Harada, "Data rate enhancement of FSK transmission scheme for IEEE 802.15.4-based field area network," *IEEE Sensors J.*, vol. 21, no. 7, pp. 9600–9611, Apr. 2021.

[6] K. Makino, K. Mizutani, T. Matsumura, and H. Harada, "Super-large-coverage standardized wireless communication system and its implementation in VHF band for IoT and V2X," *IEEE Open J. Veh. Technol.*, vol. 4, pp. 667–680, 2023.

[7] J. Lim, K. Nakura, and H. Harada, "Super-large coverage IEEE 802.15.4g-FSK-based wireless IoT system in VHF-band," in *Proc. 2023 IEEE 9th World Forum Internet Things*, Aveiro, Portugal, 2023, pp. 1–6.

[8] R. Ouyang, T. Matsumura, K. Mizutani, and H. Harada, "Software-defined radio-based evaluation platform for highly mobile IEEE 802.22 system," *IEEE Open J. Veh. Technol.*, vol. 3, pp. 167–177, 2022.

[9] S. Mori, K. Mizutani, and H. Harada, "Software-defined radio-based 5G physical layer experimental platform for highly mobile environments," *IEEE Open J. Veh. Technol.*, vol. 4, pp. 230–240, 2023.

[10] K. Nakura, S. Mori, H. Masaki, and H. Harada, "Software-defined radio-based IEEE 802.15.4 SUN OFDM evaluation platform for highly mobile environments," *IEEE Open J. Veh. Technol.*, vol. 5, pp. 95–107, 2024.

[11] K. Obata, K. Mizutani, and H. Harada, "Carrier frequency offset estimation scheme for IEEE 802.15.4g based wide area WI-SUN systems," in *Proc. IEEE Int. Conf. Commun.*, 2016, pp. 1–6.

[12] G. S. da Silva, E. R. de Lima, and C. G. Chaves, "Using maximal ratio combining and subcarrier selection to improve the OFDM receiver performance in IEEE802.15.4g," in *Proc. 2016IEEE 27th Annu. Int. Symp.*, Valencia, Spain, 2016, pp. 1–6.

[13] G. R. K. Sai Teja and P. Samundiswary, "Performance analysis of DYMO protocol for IEEE 802.15.4 based WSNs with mobile nodes," in *Proc. 2014 Int. Conf. Comput. Commun. Inform.*, Coimbatore, India, 2014.

[14] F. Bashir, W.-S. Baek, P. Sthapit, D. Pandey, and J.-Y. Pyun, "Coordinator assisted passive discovery for mobile end devices in IEEE 802.15.4," in *Proc. 2013 IEEE 10th Consum. Commun. Netw. Conf.*, Las Vegas, NV, USA, 2013, pp. 601–604.

[15] A. Vasileiadis and A. C. Iossifides, "Performance of high rate 802.15.4 UWB PHY over multipath fading channels," in *Proc. 2016 23rd Int. Conf. Telecommun.*, Thessaloniki, Greece, 2016, pp. 1–6.

[16] S. Wang, A. Huang, and T. Zhang, "Performance evaluation of IEEE 802.15.4 for V2V communication in VANET," in *Proc. 2013 Int. Conf. Comput. Inf. Sci.*, Shiyang, China, 2013, pp. 1603–1606.

[17] R. Hirakawa, R. Okumura, K. Mizutani, and H. Harada, "A novel routing method with load-balancing in Wi-SUN FAN network," in *Proc. 2021 IEEE 7th World Forum Internet Things*, New Orleans, LA, USA, 2021, pp. 362–367.

[18] K. Obata, K. Mizutani, and H. Harada, "Symbol synchronization scheme for wide area M2M wireless communication systems," *IEICE Tech. Rep.*, vol. 115, no. 189, pp. 71–76, Aug. 2015.

[19] K. Mochizuki, K. Mizutani, and H. Harada, "FFT based high-efficient receiver for FSK packet transmission systems," *IEICE Tech. Rep.*, vol. 115, no. 74, pp. 119–124, Mar. 2016.

[20] "Signal analyzer MS2830A," *Anritsu*, May 2022. [Online]. Available: https://dl.cdn-anritsu.com/en-en/test-measurement/files/Product-Introductions/Product-Introduction/ms2830a-el1-1700.pdf

[21] "PXIe-6674T specifications," NI, May–Jul 2022. [Online]. Available: https://www.ni.com/docs/ja-JP/bundle/pxie-6674t-specs/page/specs.html

[22] "NI 5791R user manual and specifications," NI, May 2013. [Online]. Available: https://www.ni.com/docs/ja-JP/bundle/373845d/resource/373845d.pdf

[23] "PXIe-7975 specifications," *NI*, 2022. [Online]. Available: https://www.ni.com/docs/ja-JP/bundle/pxie-7975-specs/resource/pxie-7975-specs.pdf

[24] ROHM, "920MHz band specified low power radio module BP3596, Datasheet," 2013.

[25] L. Schmitt, T. Grundler, C. Schreyoegg, I. Viering, and H. Meyr, "Maximum ratio combining of correlated diversity branches with imperfect channel state information and colored noise," in *Proc. 8th IEEE Int. Symp. Spread Spect. Tech. App. – Prog. Book Abst.*, Sydney, NSW, Australia, 2004, pp. 859–863.

[26] D. G. Brennan, "Linear diversity combining techniques," *Proc. IRE*, vol. 47, no. 6, pp. 1075–1102, Jun. 1959.

[27] H. Harada and R. Prasad, *Simulation and Software Radio For Mobile Communications*. Norwood, MA, USA: Artech House, 2002.

[28] European Commission, "Directorate-General for the information society and media, COST 207 – digital land mobile radio communications," Beaulieu, Belgium, Mar. 1989.

[29] E. Sofer and G. Chouinard, "WRAN channel modeling," *IEEE Standard 802.22-05/0055r7*, Aug. 2005.

[30] H. Harada, "Fundamental field experiments of OFDMA systems using VHF-band in urban area," in *Proc. 2023 26th Int. Symp. Wireless Pers. Multimedia Commun.*, Tampa, FL, USA, 2023, pp. 154–158.

[31] M. Hata, "Empirical formula for propagation loss in land mobile radio services," *IEEE Trans. Veh. Tech.*, vol. VT-29, no. 3, pp. 317–325, Aug. 1980.

[32] H. Harada, S. Mori, and K. Miztani, "Performance evaluation of 5G in VHF band for super-large coverage communication systems," in *Proc. IEEE Conf. Standards Commun. Netw.*, Thessaloniki, Greece, 2022, pp. 212–217.

JAESEOK LIM is received the B.E. degree in electric and electrical engineering in 2023 from Kyoto University, where he is currently working toward the M.I. degree with the Graduate School of Informatics. His research focuses on physical layer technologies of a wireless smart utility network (Wi-SUN).

KEITO NAKURA received the B.E. degree in electric and electrical engineering from Kyoto University, Japan, in 2022, and the M.I. degree from the Graduate School of Informatics, Kyoto University, in 2024. His research focuses on physical layer technologies of a wireless smart utility network (Wi-SUN).

SHOTA MORI (Member, IEEE) received the B.E. degree from the Faculty of Engineering, Kyoto University, Japan, in 2021, and the M.I. and Ph.D. degrees from the Graduate School of Informatics, Kyoto University, in 2023 and 2024, respectively. His research topics include physical layer technologies of 6th generation mobile communication (6G) system. He was the recipient of the Student Paper Award from IEEE VTS Tokyo/Japan Chapter in 2021 and the Student Award from IEICE technical committee on SRW in 2022.

HIROSHI HARADA (Senior Member, IEEE) is currently a Professor of the Graduate School of Informatics, Kyoto University, Japan, and a Research Executive Director of Wireless Networks Research Center, National Institute of Information and Communications Technology (NICT). He joined the Communications Research Laboratory, Ministry of Posts and Communications, in 1995 (currently, NICT). He was a Visiting Professor with the University of Electro-Communications, Tokyo, Japan, from 2005 to 2014. Since 1995, he has researched software defined radio, cognitive radio, dynamic spectrum access network, wireless smart ubiquitous network, and broadband wireless access systems on VHF, UHF, microwave, and millimeter-wave bands. In 2014, he was a Professor with Kyoto University. He has also joined many standardization committees and forums in the United States as well as in Japan and fulfilled important roles in them, especially IEEE 1900 and IEEE 802. He was the Chair of IEEE DySpan Standards Committee and a Vice Chair of IEEE 802.15.4g, IEEE 802.15.4m, 1900.4, and TIA TR-51. He was a Board of Directors of IEEE communication society standards board, SDR forum, DSA alliance, and WhiteSpace alliance. He is a Co-Founder of Wi-SUN alliance and has was the Chairman of the board from 2012 to 2019 and 2024. He is currently the Vice Chair of IEEE 2857, IEEE 802.15.4aa, and IEEE 802.15.4ad. He was the Chair of the IEICE Technical Committee on Software Radio (TCSR) and the Chair of Public Broadband Mobile Communication Development Committee, ARIB. He is also involved in many other activities related to telecommunications. He authored the book titled "*Simulation and Software Radio for Mobile Communications (Artech House, 2002)*." He was the recipient of the achievement awards in 2006 and 2018 and Fellow of IEICE in 2009, respectively and the achievement awards of ARIB in 2009, 2018, and 2022, respectively, on the topic of research and development of cognitive radio and Wi-SUN.